"Computational fluid dynamics simulation of two-phase flow and dissolved oxygen in a wastewater treatment oxidation ditch"

Dr Tom Matko

University of Bath, UK

Bournemouth University, UK

Prof Jan Hofman

Prof Jian Chang

Prof John Chew

Dr Jannis Wenk

29th of July, 2020

Abstract

This paper presents a computational fluid dynamics (CFD) model of an aerated wastewater treatment oxidation ditch, taking into account gas-liquid flow, mass transfer and dissolved oxygen. This innovative study contributes to knowledge as it considers the effect of bubble size distribution (BSD) and biochemical oxygen demand (BOD) distribution on the dissolved oxygen (DO) distribution. Species transport modelling predicts the DO and BOD distribution. De-oxygenation of local dissolved oxygen by BOD is modelled by an oxygen sink that depends on the local BOD concentration. Bubble coalescence and breakup models predict the BSD. The behaviour of the ditch is non-ideal, which is indicated by the residence time distribution (RTD) and the heterogeneous flow pattern and DO distribution. The parameters with the greatest influence on the dissolved oxygen are the BOD and bubble size. There is good agreement with the observed flow patterns and the measurements of mean DO. This study identifies that the BOD distribution and the BSD are important parameters for predicting the dissolved oxygen distribution and are also current gaps in the published research.

KEYWORDS: Aeration; Oxidation ditch; Computational fluid dynamics; Dissolved oxygen; Multiphase flow; Wastewater treatment

1. Introduction

Aeration can be as much as 45 - 90 % of the energy cost of a wastewater treatment plant (Rosso et al., 2008). Aeration increases the dissolved oxygen and enables chemical and biological oxidation (Thakre et al., 2008). Dissolved oxygen (DO) allows the aerobic bacteria to remove the biochemical oxygen demand (BOD). An oxidation ditch (OD) is a closed-loop open channel with horizontal surface impellers that circulate flow within a 'racetrack' (Potier et al., 2005). Ditches are widely used due to their high BOD, phosphorus and nitrogen removal (Yang *et al.,* 2010). However they have a bend geometry, shallow depth and aeration that encourage undesirable heterogeneous distribution (Karpinska and Bridgeman, 2016).

Mechanical surface aeration is the oxygen transfer through the water surface by surface agitation (McWhirter et al., 1995). Diffusion aeration is the oxygen transfer from a submerged source (Karpinska et al., 2010). Fine pore membrane diffusers produce the smallest bubbles (Rosso et al., 2008). The mixing impeller provides contact between biomass and the nutrients and encourages desirable homogeneous distribution (Karpinska et al., 2010). The aeration performance also depends on the hydraulic residence time (Potier et al., 2005). Oxygen transfer through the water surface is usually considered negligible compared to the bubble surface area (Hu et al., 2010). There is more information on aeration in the literature (Karpinska, 2013).

Computational Fluid Dynamics (CFD) can predict the multi-phase flow pattern, dissolved oxygen distribution (Karpinska and Bridgeman, 2016) and aeration performance of a wastewater aeration tank (Samstag et al., 2016). Smaller bubbles increase the oxygen mass transfer by increasing the interfacial gas-liquid bubble surface area (Karpinska and Bridgeman, 2016). One common simplifying assumption is a uniform bubble size (Lei and Ni, 2014). Bubble coalescence is therefore sparingly addressed (Climent et al., 2019; Dhanasekharan et al., 2005; Karpinska and Bridgeman, 2018). However, studying the effect of bubble size distribution (BSD) on dissolved oxygen is recommended (Le Moullec et al., 2010).

Species transport modelling can predict the oxygen mass transfer and the distribution of DO (Karpinska and Bridgeman, 2016). The oxygen scalar equation includes a source term for aeration (Huang et al., 2009). There is a sink term for the consumption of oxygen by BOD (Yang et al., 2011). The BOD concentration is commonly simplified as homogeneous in the aeration tank (Littleton et al., 2007). However, it is recommended that the BOD distribution is modelled as a heterogenous oxygen sink (Ghawi et al., 2014; Karpinska and Bridgeman, 2018). The ideal oxidation ditch has a uniform flow pattern (Liu et al., 2014), uniform DO distribution (Yang et al., 2011), uniform solids distribution (Xie et al., 2014), high dissolved oxygen (Karpinska and Bridgeman, 2018), high residence time (Wei et al., 2016) and low energy cost (Zhang et al., 2016).

This study takes into account gas-liquid flow, fluid turbulence, inter-phase oxygen mass transfer, bubble drag force, bubble coalescence and BOD distribution. The CFD model can predict the flow pattern and DO distribution in a full-scale wastewater oxidation ditch. The CFD model can predict the dissolved oxygen more accurately as it considers the BSD and BOD distribution. De-oxygenation of the local dissolved oxygen by BOD is modelled by an oxygen sink that depends on the local BOD. This is a novel approach to flow modelling. Predictions are also evaluated by comparison between computation and on-site experimentation. Three phase flow behaviour is ignored due to the complexity of the suspended solids. This study identifies that the BOD distribution and the BSD are important parameters. It identifies ways in which the CFD model can be improved. It considers how the CFD model can improve the design of the oxidation ditch and the aeration devices.

This study identifies the factors that affect the uniformity of the flow pattern and dissolved oxygen distribution and the level of the dissolved oxygen. There are different aeration devices (surface, membrane diffuser, hydro-jet and air jet). The energy cost of an aeration device depends on its water, air and power requirements (Stenstrom and Rosso, 2010). Aeration devices are competitively bid on the basis of oxygen transfer per unit of power (Thakre et al., 2008). The conversion of the energy cost into dissolved oxygen can be evaluated in a CFD simulation (Thakre et al., 2008). The CFD model will be used in the future by the company Wessex Water for the design and energy costing of their aeration systems.

Nomenclature

a	specific interfacial area, m^2
BOD	biochemical oxygen demand concentration, mg/L
BOD_{inf}	biochemical oxygen demand influent concentration, mg/L
BOD_{load}	biochemical oxygen demand influent mass flow rate, kg/s
BOD_{sink}	biochemical oxygen demand sink, kg/s
BSD	bubble size distribution
C_0	initial dissolved oxygen concentration in aeration tank, mg/L
C_d	drag coefficient of spherical bubbles in pure liquid
C_{DS}, C_L^*	saturation dissolved oxygen concentration in water, kg/m^3
C_L	dissolved oxygen concentration in water, kg/m^3
CFD	computational fluid dynamics
C_s	scalar/species concentration, kg/m^3
d_b	bubble diameter, m
D_m	mass diffusivity, m^2/s
D_o	standard mass diffusivity of oxygen at 20 ºC, m^2/s
DO	dissolved oxygen concentration, mg/L
DO_{load}	dissolved oxygen influent mass flow rate, kg/s
DO_{sink}	dissolved oxygen sink, kg/s
$\overrightarrow{F_q}$	interfacial forces between phases, N
g	gravitational acceleration, ms^{-2}
H^x	Henry coefficient, Pa
HRT	hydraulic residence time, s
k	velocity scale turbulent kinetic energy, m^2s^2
K_L	local mass transfer coefficient, m/s
K_La	overall / oxygen mass transfer coefficient, s^{-1}, h^{-1}
L_k	interfacial transfer of oxygen between phases, kg/m^3s
$\dot{m}_{pq}$, $\dot{m}_{qp}$	mass transfer from phase p to q and from phase q to p, kg/s
MRF	multiple reference frame
MUSIG	multiple size group

OD	oxidation ditch
OTR	oxygen transfer rate, mg/h
p	pressure, N/m^2
P_{Ag}	partial pressure of component A in gas phase, Pa
PBM	population balance model
PSD	particle size distribution
RANS	Reynolds averaged Navier-Stokes
Re_m	mixture Reynolds number
RTD	residence time distribution
Sc_t	turbulent Schmidt number
t	time, s
T	temperature, $^{\circ}C$
u_g	gas velocity, m/s
u_l	liquid velocity, m/s
V	tank fluid volume, m^3
VOF	volume of fluid
$\overrightarrow{v_q}$	effective velocity, m/s
WWTP	wastewater treatment plant
X_{Al}	mole fraction of component A in liquid phase

Greek letters

$\alpha_q \, \rho_q$	effective density of phase q, kg/m^3
μ_m	mixture viscosity, kg/ms
μ_t	turbulent viscosity, kg/ms
μ_q	shear viscosity of phase q, kg/ms
α_g	gas volume fraction
α_q	volume fraction of phase q
ε	turbulence length scale eddy dissipation rate, m^2/s^3
ρ	density, kg/m^3
ρ_l	liquid water density, kg/m^3
ρ_q	density of phase q, kg/m^3

2.   Materials and methods

2.1   Physical properties

The physical properties (Table 1) are at the mean annual ambient temperature of 13 °C at the wastewater treatment plant (Çengel and Boles, 2008). The dry oxygen occupies around 21% by volume of dry air. The standard mass fraction of oxygen in air is 0.232 at 1 atm pressure and at 20 °C (Degremont, 2007). Oxygen has a higher density and viscosity than air (Çengel and Boles, 2008). The saturation dissolved oxygen concentration in water is equivalent to a volume fraction of air in water of 0.036 (Degremont, 2007). The mass diffusion coefficient of oxygen in air is 1.26×10^{-5} m^2/s and in water is 1.2×10^{-9} m^2/s (Çengel and Boles, 2008).

Table 1 – Physical properties.	
Temperature (°C)	13
Density of water (kg/m^3)	999.4
Density of air (kg/m^3)	1.233
Density of oxygen (kg/m^3)	1.370
Viscosity of water (kg/ms)	0.0012
Viscosity of air (kg/ms)	0.0000179
Viscosity of oxygen (kg/ms)	0.0000201
Bubble diameter (mm)	4
Mass fraction of oxygen in air	0.233
Saturation of air in water (volume fraction)	0.036
Saturation of dissolved oxygen in water (mg/L)	10.5
Mass diffusivity of oxygen in air (m^2/s)	1.26×10^{-5}
Mass diffusivity of oxygen in water (m^2/s)	1.2×10^{-9}
Turbulent Schmidt number of oxygen in air	0.7
Turbulent Schmidt number of oxygen in water	0.7
Molar concentration Henry coefficient (Pa.m^3/mol)	61636
Molar fraction Henry coefficient (Pa)	3.4×10^9
Mass transfer coefficient of surface aeration (h^{-1})	3

2.2 Mathematical modelling

2.2.1 Two phase flow

The multi-fluid model is the most commonly used multi-phase flow model for the large bubble population in an aeration tank (Höhne and Mamedov, 2020; Hreiz et al., 2019; Karpinska and Bridgeman, 2016; Karpinska and Bridgeman, 2018). It solves the continuity and momentum equations of each phase (Ranade, 2002).

Mass conservation equation (Ratkovich, 2010):

$$\frac{\partial}{\partial t}\left(\alpha_q \rho_q\right) + \nabla \cdot \left(\alpha_q \, \rho_q \, \overrightarrow{v_q}\right) - \sum_{p=1}^{n}\left(\dot{m}_{pq} - \dot{m}_{qp}\right) = 0 \qquad (1)$$

where ρ_q is density, term $\alpha_q \, \rho_q$ is effective density of phase q, $\overrightarrow{v_q}$ denotes its velocity, $\dot{m}_{pq}$ and $\dot{m}_{qp}$ are mass transfer mechanisms from phase p to q and from q to p.

Momentum conservation equation (Ratkovich, 2010):

$$\frac{\partial}{\partial t}\left(\alpha_q \, \rho_q \, \overrightarrow{v_q}\right) + \nabla \cdot \left(\alpha_q \, \rho_q \, \overrightarrow{v_q} \, \overrightarrow{v_q}\right) = -\alpha_q \, \Delta p + \nabla \cdot \mu_q \left(\nabla \, \alpha_q \, \overrightarrow{v_q} + \nabla \, \alpha_q \, \overrightarrow{v_q} \, T\right) + \rho_q \, \overrightarrow{g} + \overrightarrow{F_q}$$

$$(2)$$

where p is the pressure shared by all phases, μ_q denotes shear viscosity of phase q, and $\overrightarrow{F_q}$ is the sum of interfacial forces between continuous and disperse phases.

Gas-liquid fluid flow is characterised by the momentum exchange inter-phase drag force. The rise velocity of the bubbles and the bubble diameter predict the drag force (Talvy et al., 2007). It uses the mixture Reynolds number (Ishii and Zuber, 1979):

$$Re_m = \rho_l \, d_b \frac{|u_g - u_l|}{\mu_m} \qquad (3)$$

where, Re_m is the mixture Reynolds number, ρ_l is liquid water density (kg/m^3); d_b is bubble diameter (m); u_g is velocity of gas phase (m/s); u_l is velocity of liquid phase (m/s), μ_m is mixture viscosity (kg/ms).

In the viscous (transitional) flow regime the drag coefficient is defined:

$$C_d = \left(\frac{24}{Re_m}\right) \left(1 + 0.1 \ Re_m{}^{0.75}\right) \qquad (4)$$

Bubble size is important for inter-phase momentum and mass transfer, as it influences the interfacial gas-liquid bubble area (Fayolle et al., 2007). One common assumption is a uniform bubble size. However, turbulent eddies cause there to be bubble coalescence and a bubble size distribution (BSD) (Nopens et al., 2015). Bubble coalescence is caused by bubble wake and rise velocity (Luo and Svendsen, 1996). Bubble size also depends on the orifice or pore size of the diffusion aerator (Wang et al., 2009), although this is not modelled in this study. A uniform mean bubble size of 4 mm in this study is taken as an average value from the literature (Lei and Ni, 2014; Le Moullec et al., 2010; Terashima et al., 2016; Xu et al., 2010).

The bubbles are modelled as a polydisperse phase (Frank et al., 2005) using the homogeneous multiple size group (MUSIG) model (Lo, 1998). The homogeneous MUSIG model is suitable for bubbly flow in an aeration tank (Frank et al, 2005). The coupling between the multi-fluid model and the coalescence model is through the inter-phase bubble drag term. The multi-fluid model that incorporates a bubble size distribution (BSD) requires a population balance model (PBM) (Climent et al, 2019; Dhanasekharan et al, 2005; Karpinska and Bridgeman, 2018). The bubble size range modelled in this ditch is 0 - 8 mm with four equal subdivisions. The effect of hydrostatic pressure on bubble size (Fayolle et al., 2006) and the deformable bubble shape (Wang et al., 2009) are ignored, which is similar to other CFD models.

2.2.2 Oxygen mass transfer

Oxygen mass transfer between the air and water phases (Fayolle et al., 2007):

$$L_k = K_L a \, (C_L^* - C_L) \tag{5}$$

where L_k is the interfacial transfer of oxygen concentration (kg/m³s). K_L is local mass transfer coefficient (m/s). The interfacial area, a, is the ratio of the total surface area of the gas bubbles to the liquid volume. The product of these terms $K_L a$ is the oxygen mass transfer coefficient (s^{-1}). C_L is the DO concentration in water (kg/m³), and C_L* is the saturation DO concentration in water at the temperature T (kg/m³). Using Higbie's film penetration theory (Higbie, 1935; Le Moullec et al., 2010):

$$K_L a = 2 \sqrt{D_o \, \frac{|u_g - u_l|}{d_b}} \, \frac{6 \, \alpha_g}{d_b} \tag{6}$$

where D_o is the standard mass diffusivity of oxygen (m²/s), d_b is bubble diameter (m), α_g is gas volume fraction, and u_g and u_l are the respective gas and liquid phase velocities (m/s). The local distributed mass transfer coefficient K_L depends on the spatial distributions of these other parameters. Oxygen mass transfer can be increased by increasing the interfacial bubble area or the driving force of the oxygen concentration (Degremont, 2007; Gillot and Heduit, 2000).

2.2.3 Two equation k-ε turbulence model

The Reynolds Averaged Navier-Stokes (RANS) equations (Launder and Spalding, 1974) model the effects of turbulence on the mean flow properties for the whole range of turbulent length scales. The standard two equation k-ε (k-epsilon) turbulence closure model (Pope, 2000) solves two additional transport equations for turbulence quantities: velocity scale turbulent kinetic energy, k, and turbulence length scale eddy dissipation rate, ε. This turbulence model is the most popular for an oxidation ditch due to its robustness, low computational cost and reasonable accuracy (Cockx et al., 2001; Fayolle et al., 2007; Lei and Ni, 2014; Xu et al., 2010; Zhang et al., 2019). The two-equation turbulence models assume isotropic turbulence (Launder and Spalding, 1974). The turbulence models are assessed in detail in the literature (Launder and Spalding, 1974; Pope, 2000; Rodi, 1993).

2.2.4 BOD and DO distribution

The species transport equation predicts the local mass fraction concentration of a scalar. Species can be coupled to the momentum equation as an equation of state, or treated as a passive property that is transported by the fluid. The species transport of a scalar concentration in turbulent flow (Ranade, 2002):

$$\frac{\partial}{\partial t} \left(\rho_l \, C_s \right) + \nabla \cdot \left(\rho_l \, U_l \, C_s \right) = \nabla \cdot \left(\left(\rho_l \, D_m + \frac{\mu_t}{Sc_{ct}} \right) \nabla \, C_s \right) \qquad (7)$$

where, C_s is the concentration of scalar (kg/m^3); U_l is statistical average velocity (m/s); D_m is mass diffusivity (m^2/s); μ_t is turbulent viscosity (kg/ms); Sc_t is turbulent Schmidt number.

For the absorption of the gas into a dissolved liquid there is an equilibrium between the two phases (Degremont, 2007). Henry's law states that the dissolved gas in a liquid is proportional to its partial pressure above the liquid. The proportionality factor is therefore Henry's law constant.

$$P_{Ag} = H^x \, X_{Al} \qquad (8)$$

where P_{Ag} is the partial pressure of component A in the gas phase (Pa), X_{Al} is the mole fraction of component A in the liquid phase, H^x is Henry coefficient (Pa).

The spatial distribution of dissolved oxygen considers the mass transport of oxygen in the air phase, interfacial mass transfer of oxygen from air to water phase, mass transport of oxygen in the water phase and absorption of oxygen into the water phase (Karpinska et al., 2015). The oxygen scalar equation includes the consumption of oxygen by BOD. This is usually addressed by a homogeneous oxygen sink throughout the ditch (Guo et al., 2013; Littleton et al., 2007; Yang et al., 2011). However, a suggested improvement in this paper is to consider the effect of BOD distribution on dissolved oxygen by modelling it as a heterogeneous oxygen sink. This is also suggested by other investigators (Karpinska and Bridgeman, 2018).

The dissolved oxygen sink in this study uses both a uniform and a distributed BOD. There is a two-way coupled relationship between DO and BOD. Higher local DO is more likely to increase the BOD degradation and result in local lower BOD (Degremont, 2007). Firstly, the spatial distribution of BOD in the water phase is predicted by using the species transport equation. Secondly, the reduction of local BOD is modelled with a distributed sink in the whole of the ditch, that is solely dependent on the local predicted mass fraction of dissolved oxygen:

$$BOD_{sink} = DO \times \frac{BOD_{load}}{BOD_{inf}} \tag{9}$$

where BOD_{sink} is the local sink term of BOD (kg/s), DO is the local predicted dissolved oxygen concentration (mg/L), BOD_{load} is the influent mass flow rate of BOD (kg/s), BOD_{inf} is the influent BOD concentration (mg/L).

Firstly, the spatial distribution of DO in the water phase is predicted by using the species transport equation. Secondly, the reduction of local DO is modelled with a distributed sink in the whole of the ditch, that is solely dependent on the local predicted mass fraction of biochemical oxygen demand:

$$DO_{sink} = BOD \times \frac{DO_{load}}{BOD_{inf}} \tag{10}$$

where DO_{sink} is the local sink term of DO (kg/s), BOD is local predicted biochemical oxygen demand concentration (mg/L), DO_{load} is influent mass flow rate of DO (kg/s).

2.3   Boundary conditions

2.3.1   Water surface

The disturbance of the water surface can be caused by wind, variable influent flow, rotation of the surface aerator and the rising bubble plume and re-circulation from the diffuser and hydro-jet aerator (Wicklein et al, 2016). However, these are often assumed to be negligible when compared to the water depth (Guo et al., 2013). In this study the water surface is planar similar to other CFD models (Climent et al., 2019; Fayolle et al., 2007; Guo et al., 2013; Karpinska et al., 2015; Lei and Ni, 2014; Yang et al., 2011; Zhang et al., 2016). It uses the 'degassing' boundary condition (Talvy et al., 2007). It only allows air to be released from the water surface from rising bubbles. It eliminates the need of a free surface model, thereby reducing the complexity and computational cost. To model the shape of the water surface the volume of fluid (VOF) model is preferred but used sparingly (Xu et al, 2018).

2.3.2   Inlets and outlets

The influent over the weir is a velocity inlet boundary condition (0.25 m/s), with its depth equal to the measured water height over the weir. The influent air content is a volume fraction of air that is equivalent to the influent DO measurement (0.08 mg/L). The effluent is an outlet pressure boundary condition. The jet aerator is an inlet velocity boundary condition (3.5 m/s) that creates additional flow. The water in the jet stream is saturated with air with a volume fraction of air of 0.036. The grid diffuser is a single surface, that is equivalent to the surface area of the open pores in the membrane tubes (Fayolle et al., 2007; Gresch et al., 2011). The inlet velocity boundary condition of the diffuser is 0.01 m/s (Zhang et al., 2016). The flow from the diffuser is pure air with a volume fraction of air of 1. Two scalars represent the oxygen in the air and water phases. The influent mass fraction of oxygen in water is equivalent to the influent DO measurement. The influent mass fraction of BOD in water is equivalent to the influent BOD measurement (300 mg/L). The mean annual influent flow rate is used, but the effect of influent flow rate is also studied. However, the flow from the hydro-jet aerator and the recirculation from the surface aerators have a more significant impact on the flow pattern than the influent weir flow.

2.3.3 Mechanical surface aerator

The multiple reference frame (MRF) model calculates the solid-liquid interaction force from the rotational mechanical surface aerator (Fan et al., 2010). It produces a directional momentum source of the water, without producing additional flow rate. The rotational speed of the drum is 70 rpm. The maximum tangential velocity predicted by the MRF model is the correct hand calculation value.

Oxygen transfer rate (OTR) of mechanical surface aeration (Huang et al., 2009):

$$OTR = K_L a \ V \ (C_{DS} - C_o) \tag{11}$$

$$0.000833 \ \frac{1}{s} \times 2000 \ m^3 \times 0.0105 \ \frac{kg}{m^3} = 0.0175 \frac{kg}{s}$$

where OTR is the oxygen transfer rate of the spray water (mg/h), $K_L a$ is the oxygen mass transfer coefficient from the air to water phase (h^{-1}), V is tank volume = 2000 m^3 and C_o is the initial DO concentration (≈ 0). C_{DS} is the saturation DO concentration at 13 $^{\circ}$C (Degremont, 2007), which is 10.5 mg/L (0.0105 kg/m^3).

There is no physical measurement of the mass transfer coefficient of the brush surface aerators. Therefore a comparison is made between literature values (Thakre et al., 2008) for different surface aerators at 70 rpm (brush rotor = 3 h^{-1}, cage rope wound rotor = 4 h^{-1}, cage fin rotor = 4.5 h^{-1}, curved blade rotor = 14 h^{-1}). A value of 3 h^{-1} is chosen for the brush surface aerator. The oxygen mass flux source is equal to the aeration capacity of the surface aerator (Yang et al., 2011). Therefore a mass flow rate of 0.0044 kg/s of oxygen from each of the four surface aerators is modelled.

2.4   Geometric model and mesh generation

The aeration devices are shown in Figure 1. The jet aerator has a submerged flow stream of saturated aerated water through two horizontal nozzles. The four Kessener brush surface aerators are located in two sets of pairs across the channel width. The diffusion aerator injects air through a grid of 32 porous membrane pipes. The modelled geometry is shown in Figure 2. The jet aerator is in the top left of Figure 2 and near the grid diffuser. The four surface aerators are modelled as partial cylinders representing only their submerged part (Brannock, 2003). The geometry of the grid diffuser is simplified by a single upward facing square inlet (top left of Figure 2), similar to other CFD models (Fayolle et al., 2007; Gresch et al., 2011). The entire top surface is the water surface. The solid surfaces are the outer walls, floor and central wall. The water depth is 1.8 m, full length of ditch is 65 m and width is 21 m.

Fig. 1 - Aeration devices.
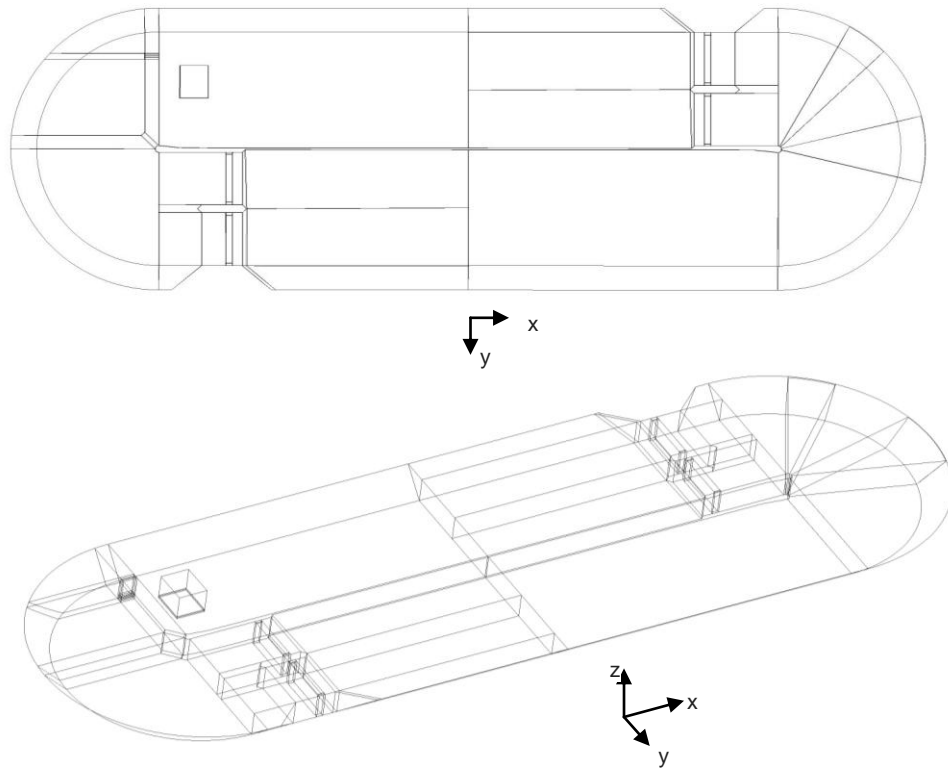
Fig. 2 - Geometric model.

The finite difference numerical method (Launder and Spalding, 1974) interpolates the computed cell centre values of the variables onto the mesh. Because of numerical accuracy there is a fully structured hexahedral mesh and second order numerical discretisation. Structured meshes are more accurate, because the grid lines are better aligned to the boundaries, which better captures the boundary layer flow. There is less numerical diffusion due to the lower cell skewness and the better orthogonality of the grid lines (Ranade, 2002). In the mesh independency study (Climent et al., 2019; Karpinska et al., 2015; Zhang et al., 2016), there is no significant difference between the flow patterns for the meshes between 206 to 698 thousand cells. For the stability of convergence of the solution the volume fraction solver solves the water and air phase equations consecutively. The under relaxation factor is lowered to 0.3 for the scalar equations to make the rate of convergence more stable. The rate of convergence is fast and converged between 3000 and 10000 iterations. The simulations are between 15 and 36 hours for the mesh with 396268 cells. The computer hardware is a 2.50 GHz processor with 16 GB RAM of memory. The simulations are speeded up by parallel processing. The well known commercial CFD software 'ANSYS-CFX' is used.

3.   Results and discussion

3.1   Water flow pattern and volume fraction distribution

Figure 3 shows the velocity vectors near the water surface without any aeration devices. Flow circulates clockwise in an almost plug flow regime. There are three recirculation zones. There is flow short circuiting from the influent to effluent that reduces the residence time. The influent has low DO and the air quickly reaches the water surface and dissipates out and there is no air in the rest of the ditch.

The ditch operates with one jet aerator, four surface aerators and one diffusion aerator. Figure 4 shows the velocities with the aeration devices. The devices increase the mean velocity in the ditch by a factor of 15. The jet aerator and surface aerators reverse the flow direction in the ditch to anti-clockwise. This is an intention of design to mitigate against short-circuiting from the influent to effluent. The jet and surface aerators create a strong flow current and there is a heterogeneous flow distribution. The upward flow from the diffuser creates a re-circulating radial flow pattern. Maximum velocities in the ditch are near the water surface: 0.34 m/s (surface aerator), 0.47 m/s (jet aerator) and 0.64 m/s (diffuser). There are small air patches just above the aerators (top of Figure 5). There is a plume of rising air from the jet aerator (middle of Figure 5). There is a stack of rising air from the diffuser (bottom of Figure 5).
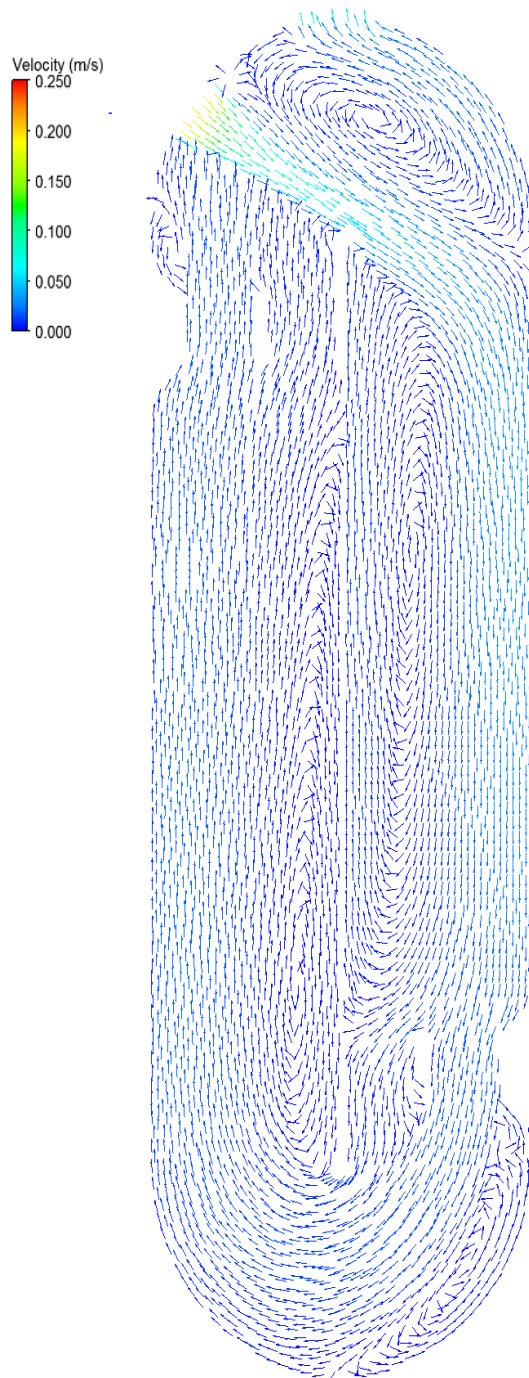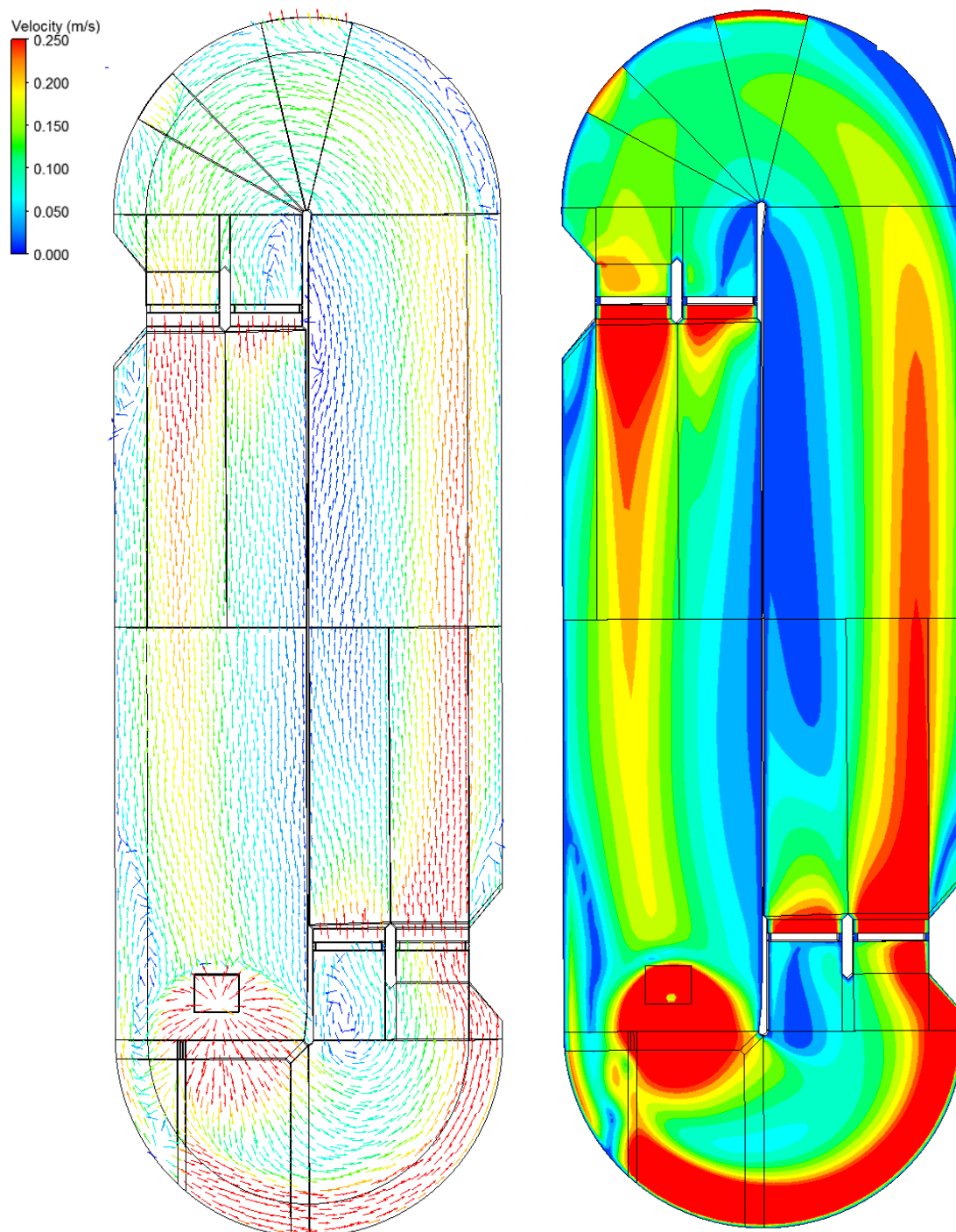
Fig. 3 - Water flow pattern without aeration devices.

Fig. 4 - Water flow pattern with aeration devices.
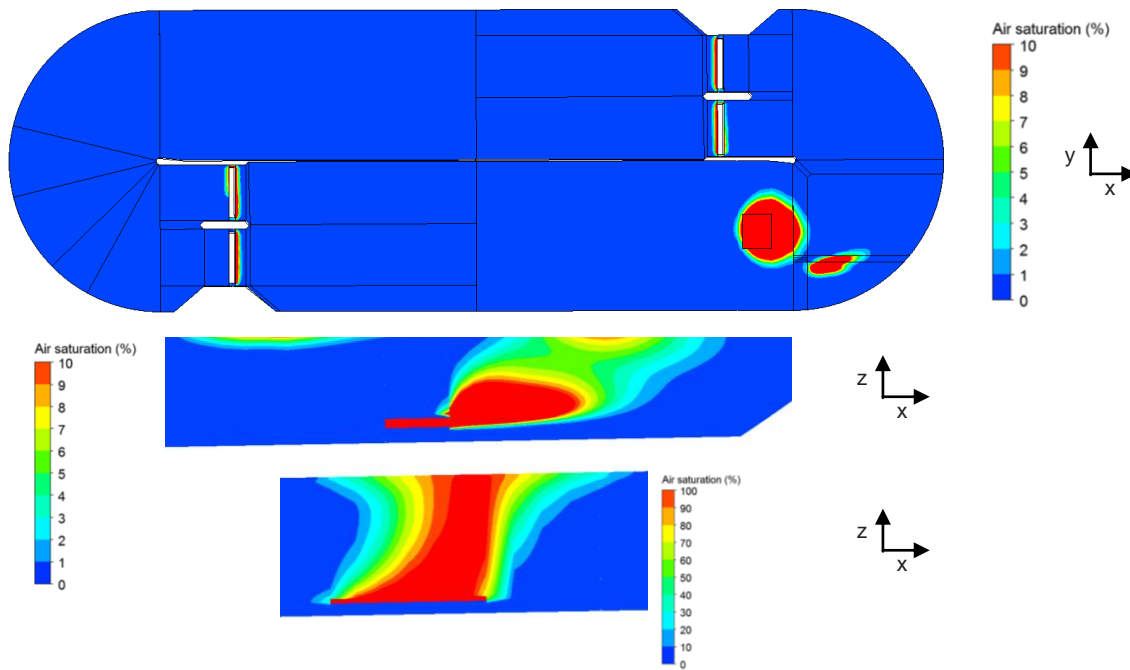
Fig. 5 - Volume fraction of air with aeration devices.

3.2 Residence time distribution

The hydraulic behaviour of the ditch can be characterised by residence time distribution (RTD) (Gresch et al., 2010; Karpinska, 2013; Nauman, 2007). The species transport of a passive tracer has the same properties as water (Le Moullec et al., 2008). The tracer concentration is measured in the effluent and this evolution with time is the RTD (Figure 6). The theoretical hydraulic residence time (HRT) is the mean residence time, which is the ditch volume divided by the mean influent flow rate (Nauman, 2007). The mass diffusivity of the tracer in water (1.35×10^{-9} m^2/s) is low enough to have no diffusive effect on the RTD (Wicklein et al., 2016). The turbulent Schmidt number of the tracer is 0.7. The most important parameter is the predicted dimensionless HRT when it is compared to the theoretical HRT. Moreover, the dimensionless time at the peak tracer concentration will determine the degree of flow short circuiting. The predicted HRT is the time at the 50 % cumulative graph area. In practical terms, this is the time when half of the mass of tracer has travelled from the influent to the effluent. The predicted HRT is 0.570 of the theoretical HRT. With the aeration devices this improves to 0.695 and the time for initial breakthrough also improves from 0.0321 to 0.0855. The devices increase the residence time and therefore improve the hydraulic efficiency of the ditch.
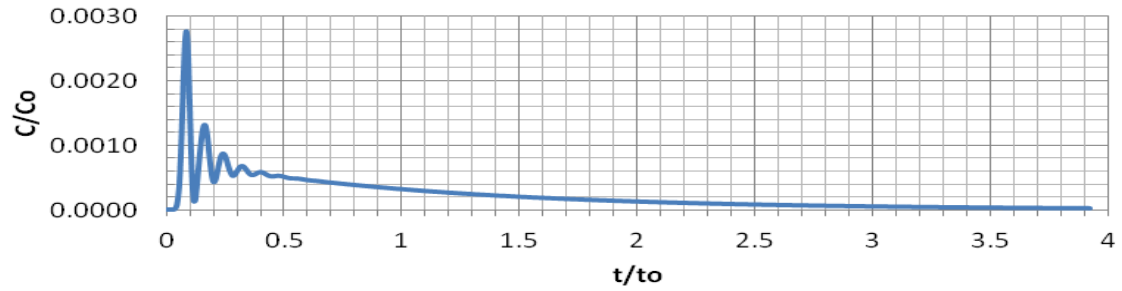
Fig. 6 - Residence time distribution of effluent with aeration devices.

3.3   BOD distribution

The BOD distribution in the ditch is not addressed in other CFD models (Guo et al., 2013; Littleton et al., 2007; Yang et al., 2011). It should not be ignored and is therefore modelled. The species transport of a passive tracer is modelled with the same properties as water (Le Moullec et al., 2008). The mass diffusivity of the BOD in water (3.5×10^{-9} m^2/s) is low enough to have no diffusive effect on the BOD. The turbulent Schmidt number of the BOD tracer is 0.7. From measurements, the mean annual influent BOD is 300 mg/L and the effluent BOD is 5 mg/L. The local sink term of the BOD in water depends only on the local DO (equation 9). The BOD distribution is adjusted by a factor in the BOD sink term to give a minimum ditch value of 0 mg/L. The BOD distribution is shown in Figure 7. It predicts a mean BOD ditch value of 15 mg/L and an effluent value of 18 mg/L. Where the local residence times are the highest (near the central wall) the BOD concentrations are the lowest.
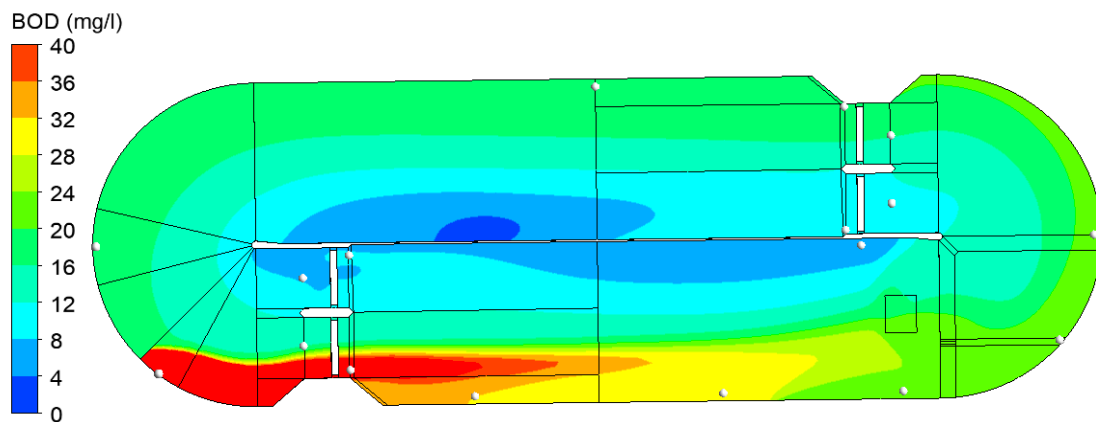

Fig. 7 - Biochemical oxygen demand distribution.

3.4 Dissolved oxygen distribution without the effect of BOD

The distribution of the dissolved oxygen is firstly predicted without the de-oxidation of BOD to only consider the effects of the aeration devices. The predicted water and air velocity distributions are quite similar. The oxygen mass fraction in the air phase predicts oxygen hotspots near the aeration sources and then it is quite evenly spread around the ditch. The inter-phase oxygen mass transfer from the air to water phase is also highest near the aeration sources (Figure 8). The mass fraction of the oxygen in the water phase is equivalent to the DO concentration. The highest DO concentrations are near the surface aerators and above the diffuser (Figure 9).
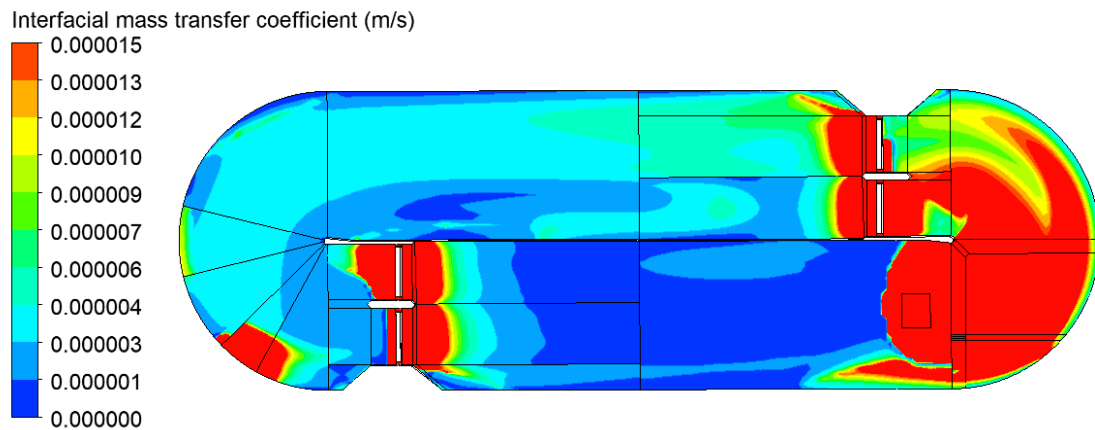

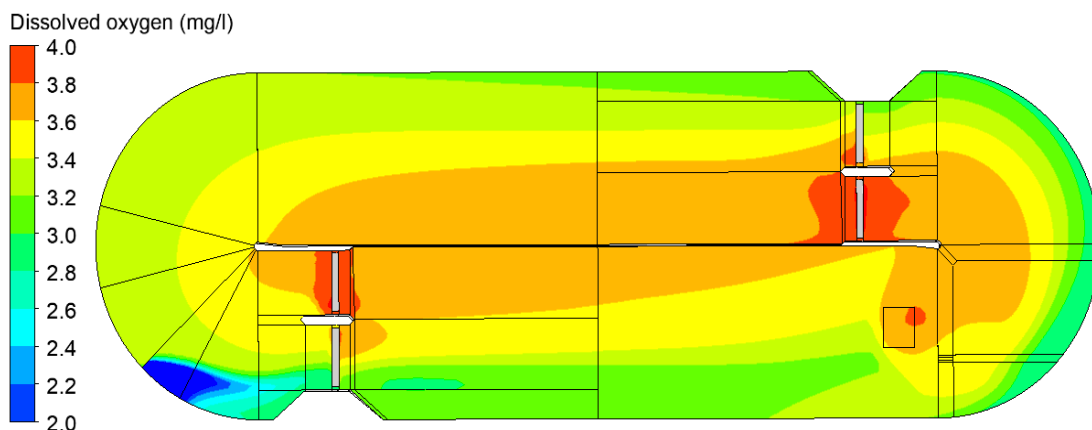**Fig. 8 - Inter-phase mass transfer coefficient.**

Fig. 9 - Dissolved oxygen without BOD.

3.5   Dissolved oxygen distribution with the effect of BOD

The uniform BOD (15 mg/L) is the mean value of the BOD distribution (Figure 7). The comparison between the uniform and distributed BOD show that the mean (0.41 and 0.42 mg/L) and maximum (1.26 and 1.24 mg/L) DO in the ditch are similar. The main difference is the variation of DO. For the uniform BOD the lowest DO is near the central wall (Figure 10). For the distributed BOD the lowest DO is downstream of the influent and near the outside wall (Figure 11). In the BOD distribution (Figure 7) the highest BOD is downstream of the influent and the lowest is near the inside wall. This result is expected by the two-way coupled relationship between DO and BOD. This is also because the highest local residence time is near the internal wall that is furthest away from the influent. An important finding of this study is that the BOD distribution has an influence on the DO distribution. Therefore a uniform BOD should not be assumed (Guo et al., 2013; Littleton et al., 2007; Yang et al., 2011).
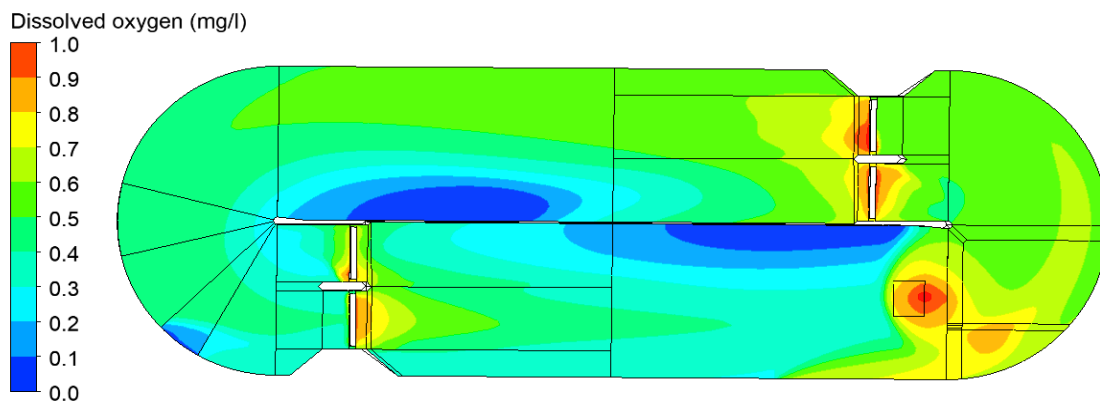

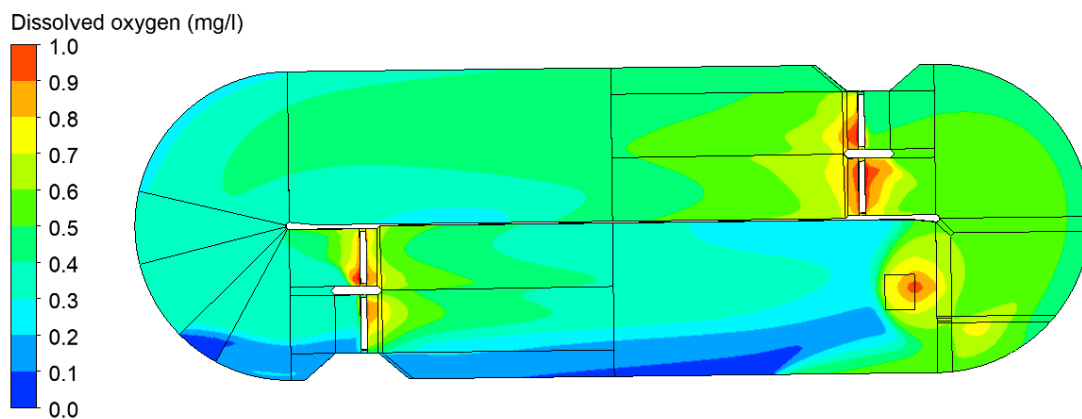**Fig. 10 - Dissolved oxygen with uniform BOD.**

Fig. 11 - Dissolved oxygen with BOD distribution.

3.6   Parameter Study

Bubbles break up and coalesce producing a bubble size distribution (BSD), which is a key parameter for oxygen mass transfer (Lei and Ni, 2014). Oxygen mass transfer can be increased by reducing bubble size, which increases the total interfacial bubble area (Fayolle et al., 2007). It can also be increased by increasing the OTR of surface aeration (Degremont, 2007). Numerous studies model a uniform bubble size (Cockx et al., 2001). However it is recommended that the effect of BSD and mass diffusivity on oxygen transfer should also be studied (Le Moullec et al., 2010).

The parameters are studied to see their effect on the DO distribution. *Table 2 shows the predicted mean and maximum DO without the effect of BOD.* In red is shown the percentage change to the mean DO in the ditch. The 'standard' model is shown in blue, and has a mean bubble size of 4 mm, physical properties at 13 $^{\circ}$C and a mass transfer coefficient of surface aeration of 3 h^{-1}. Summer conditions at 20 $^{\circ}$C are also simulated with different physical properties. A fourfold increase to 12 h^{-1} for surface aeration is also simulated. Different mean bubble sizes (3, 2, 1 mm) and a BSD are also simulated. Parameters that have an effect on the DO are temperature, mean bubble size, BSD, surface aeration, molar fraction Henry coefficient, mass diffusivity and turbulent Schmidt number of oxygen in water (Table 2).

Table 2 – Effect of parameters on dissolved oxygen without BOD.						
Parameter	Values	Mean mass transfer ($\times 10^{-5}$ m/s)	Mean DO (mg/L)	Max DO (% saturation)	Mean DO (% saturation)	Δ Mean DO (% saturation)
'Standard' (13 ° C)	properties	1.119	3.46	39	33	-
Summer (20 ° C)	properties	1.084	3.43	45	38	+5
Surface aeration (h^{-1})	12	1.125	3.90	46	37	+4
Bubble diameter (mm)	3	1.274	4.44	50	42	+9
Bubble diameter (mm)	2	1.476	5.72	64	55	+22
Bubble diameter (mm)	1	1.783	7.23	78	69	+36
Bubble size distribution (BSD) (mm)	1→6.3	1.387	3.15	37	30	-3
Molar fraction Henry coefficient (Pa)	6.8×10^{9} / 1.7×10^{9}	-	1.74 / 6.81	20 / 78	17 / 65	+16 / +32
Mass diffusivity of oxygen in water (m^{2}/s)	2.4×10^{-9} / 0.6×10^{-9}	-	4.23 / 2.75	48 / 31	40 / 26	+7 / -7
Turbulent Schmidt of oxygen in water	1.4 / 0.35	-	3.54 / 3.31	41 / 37	34 / 32	+1 / -1

The DO distribution for the parameters studied includes the effect of the BOD distribution (Figure 7). Comparing the summer (20 °C) and annual mean conditions (13 °C), the mean and maximum DO are quite similar. When the surface aeration is increased fourfold there is an increase in maximum DO to 1.77 mg/L. The dissolved oxygen near the surface aerators increase the most. When the mean bubble size is reduced to 3 mm, the maximum DO increases to 1.62 mg/L. For a 2 mm bubble size it increases further to 2.32 mg/L. For a 1 mm bubble size it increases even further to 3.64 mg/L (Figure 12). The increase in total interfacial bubble surface area for a reduced mean bubble size does increase the inter-phase oxygen mass transfer (Karpinska and Bridgeman, 2016).

Modelling BSD reduces the maximum DO only slightly from 1.24 to 1.21 mg/L. BSD does not have a significant effect on flow pattern, but it does increase the inter-phase mass transfer by 24 %, as it increases the overall interfacial bubble area (Table 2). The range of bubble sizes in the ditch is from 0.99 to 6.32 mm with a mean of 1.94 mm (Figure 13). The largest bubbles are close to the aerators and the central wall. The DO distribution for the BSD (Figure 14) shows a slight difference when compared to a uniform bubble size (Figure 11). When doubling the mass diffusivity of the oxygen in water this increases the maximum DO to 1.53 mg/L. When halving the molar fraction Henry coefficient this increases the maximum DO to 2.07 mg/L.
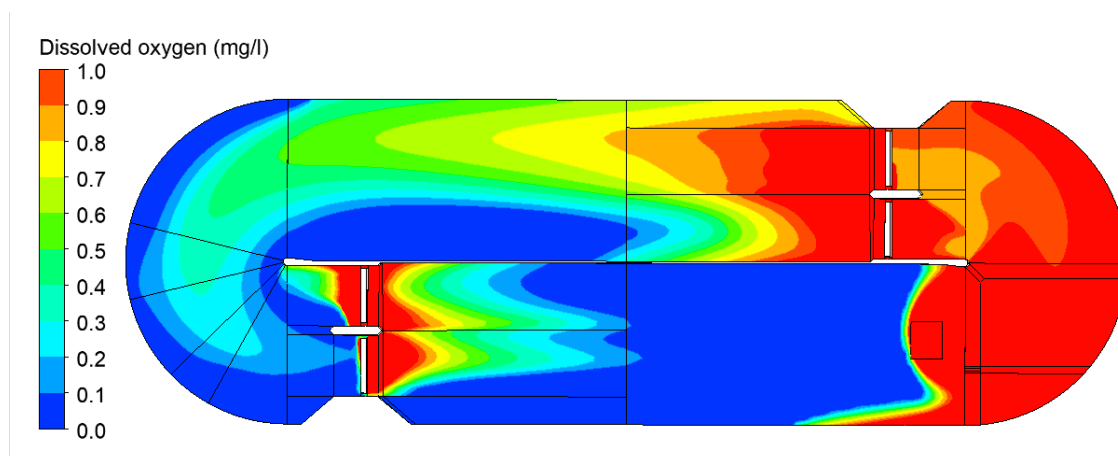

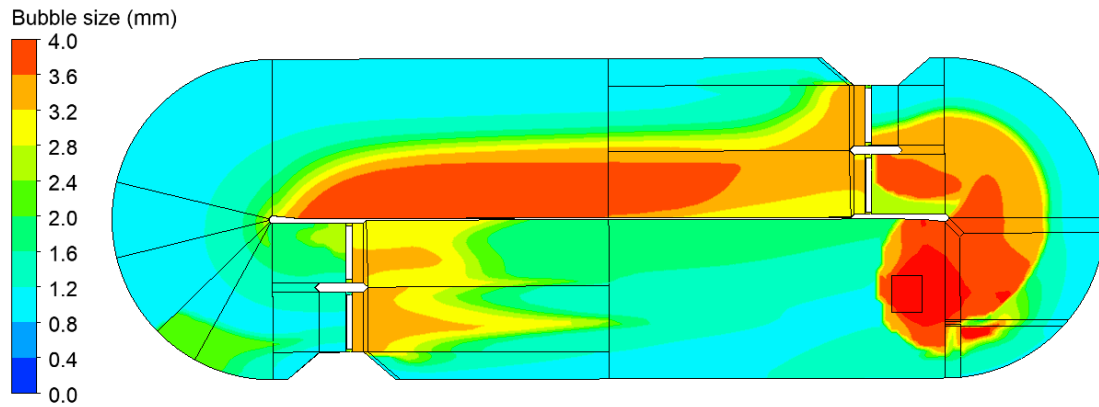**Fig. 12 - Dissolved oxygen with BOD distribution - bubble = 1 mm.**
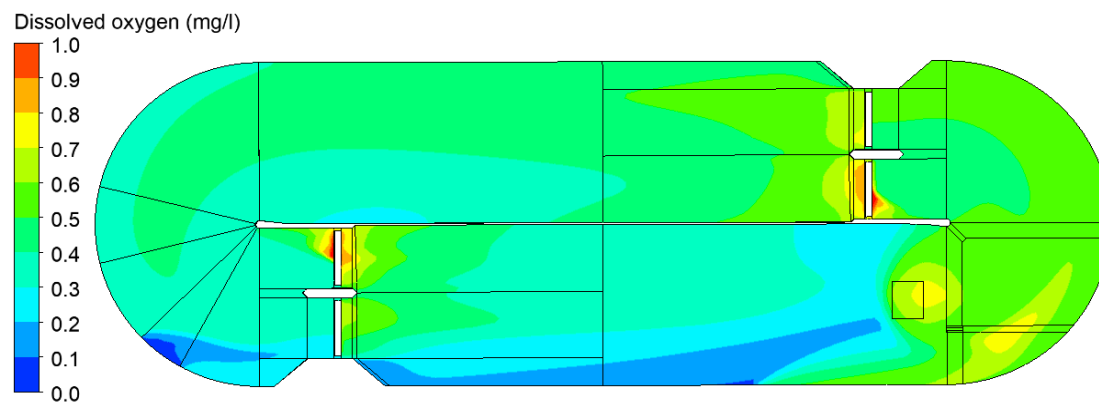
Fig. 13 - Bubble size distribution (BSD).

Fig. 14 - Dissolved oxygen with BOD distribution and BSD.

3.7   Comparison between CFD and experimental

The experiments are conducted at the wastewater treatment plant in August 2018. The temperature is measured at 20 °C. At this higher temperature the saturation concentration of dissolved oxygen is reduced to 9.1 mg/L. The flow patterns are observed by sketches, photographs and videos. The DO measurements are taken at 17 locations near the water surface with a portable optical DO meter (Hach[TM]). The measurement technique is the luminescence DO method (LDO) (Roman and Felseghi, 2014). The comparison with experimental data is only feasible when the dissolved oxygen includes the effects of the BOD.

3.7.1 Flow pattern

There is generally agreement between the prediction and experimental observation for the following fluid phenomena (Figure 15). The flow direction around the ditch is anti-clockwise. There is stagnant flow near the effluent weir, upstream of the surface aerators, upstream of the diffuser and near the central wall. There is a radial flow pattern above the diffuser. Downstream of the jet aerator there is a strong flow current, return flow along the right outer wall and fluid turbulence. There is higher flow observed downstream of the surface aerators and near the influent.
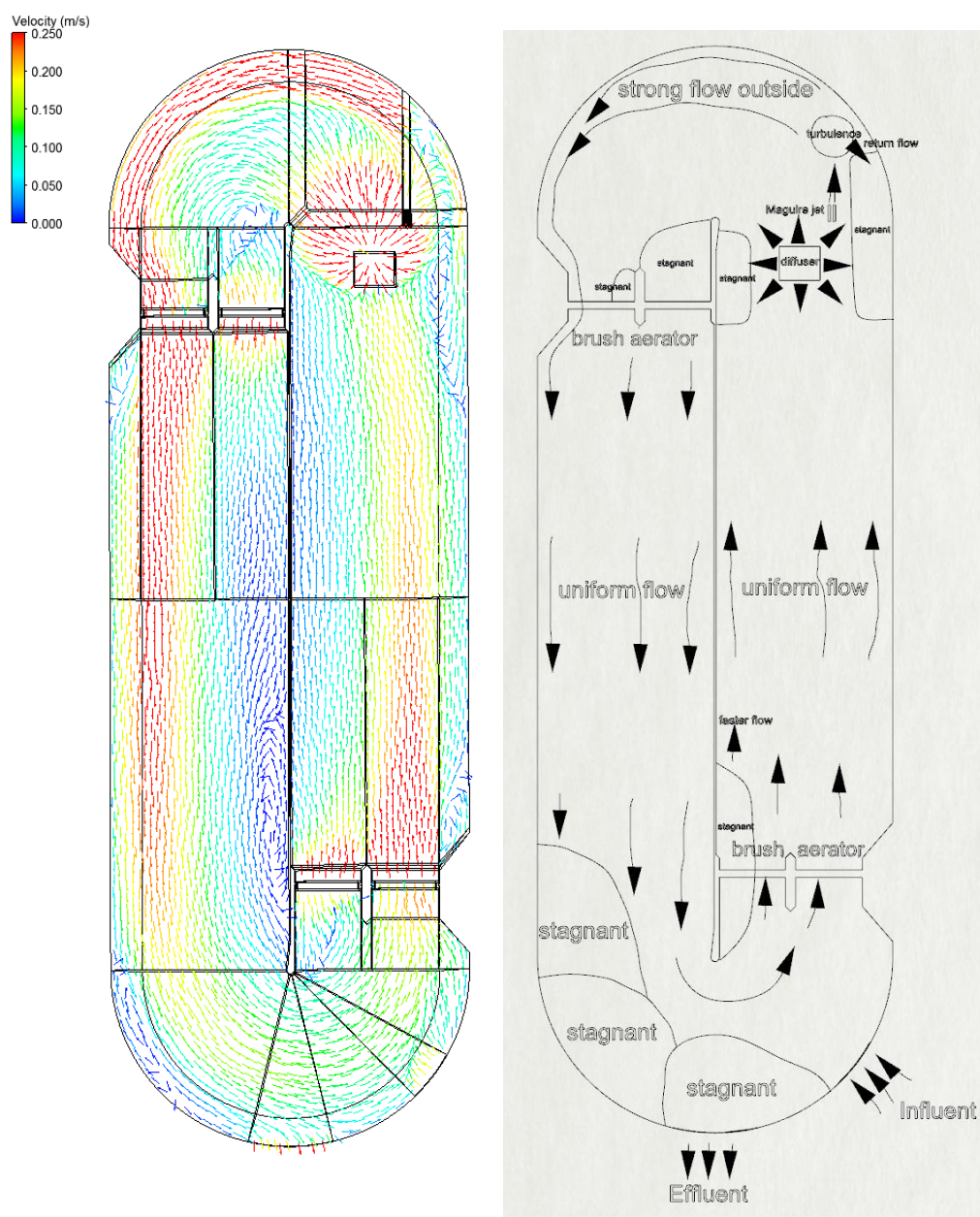

Fig. 15 - Calculated water flow pattern (left) and physical observation (right).

3.7.2 Dissolved oxygen

The comparison between the predicted mean DO in the ditch and the physical measurements are generally favourable (Table 3). The comparison for the variation of DO in the ditch is not as favourable (Table 3). *For a uniform BOD* the mean DO is in good agreement. The maximum and variation of DO in the ditch are lower than the measurements. Lowering the bubble size to 2 mm gives a mean DO that is higher than the measurements. The maximum DO and the variation of DO is nearest to the measurements for a 2 mm bubble (Table 3). The BSD gives a mean DO that is nearer to the measurements when compared to a mean bubble size of 4 mm. The maximum DO and variation of DO are still quite similar to a mean bubble size. As the bubble size is reduced, the mean and maximum DO increases due to the higher bubble interfacial area. This causes the variation of DO to increase (Figure 16).

With the BOD distribution, the variation of DO compares better with the measurements than with a uniform BOD. The closest match to the measurements is a 2 mm bubble and a BOD distribution (Table 3). An important finding is that the BOD distribution is more accurate than a mean BOD when comparison is made with experimental data. The BSD predicts a range of bubble sizes in the ditch from 1.0 to 6.3 mm with a mean of 1.9 mm (Figure 13). This compares favourably with the best match with experiment, suggesting that 2 mm could be the mean bubble size in the ditch. The BOD distribution and the BSD addressed in this study are important parameters for predicting the DO distribution. Unfortunately, in the literature there is no previous study of BOD distribution and little previous study of BSD for the CFD modelling of aeration tanks (Climent et al., 2019; Dhanasekharan et al., 2005; Karpinska and Bridgeman, 2018).

| Statistic	Measure	'Standard' model	Bubble (3 mm)	Bubble (2 mm)	Bubble (1 mm)	Bubble size distribution	Temperature (20 °C)	Surface aeration (12 h^{-1})
Table 3 – Calculated vs. measured dissolved oxygen (mg/l).								
Uniform BOD								
Mean points	0.44	0.51	0.48	0.55	0.62	0.49	0.43	0.46
Maximum points	1.38	0.76	0.84	1.15	1.67	0.70	0.68	0.71
Minimum points	0.06	0.02	0	0	0	0.04	0	0
SD points	0.44	0.20	0.23	0.36	0.63	0.19	0.17	0.17
Mean ditch	-	0.40	0.38	0.39	0.38	0.40	0.37	0.39
Maximum ditch	-	1.26	1.64	2.34	3.58	1.12	1.24	1.86
Minimum ditch	-	0	0	0	0	0	0	0
Distributed BOD								
Mean points	0.44	0.46	0.49	0.58	0.80	0.45	0.45	0.46
Maximum points	1.38	0.78	0.93	1.23	1.79	0.72	0.78	1.03
Minimum points	0.06	0.07	0	0	0	0.12	0.05	0
SD points	0.44	0.20	0.28	0.40	0.64	0.17	0.20	0.28
Mean ditch	-	0.42	0.40	0.40	0.40	0.40	0.40	0.40
Maximum ditch	-	1.24	1.62	2.32	3.64	1.21	1.25	1.77
Minimum ditch	-	0	0	0	0	0	0	0
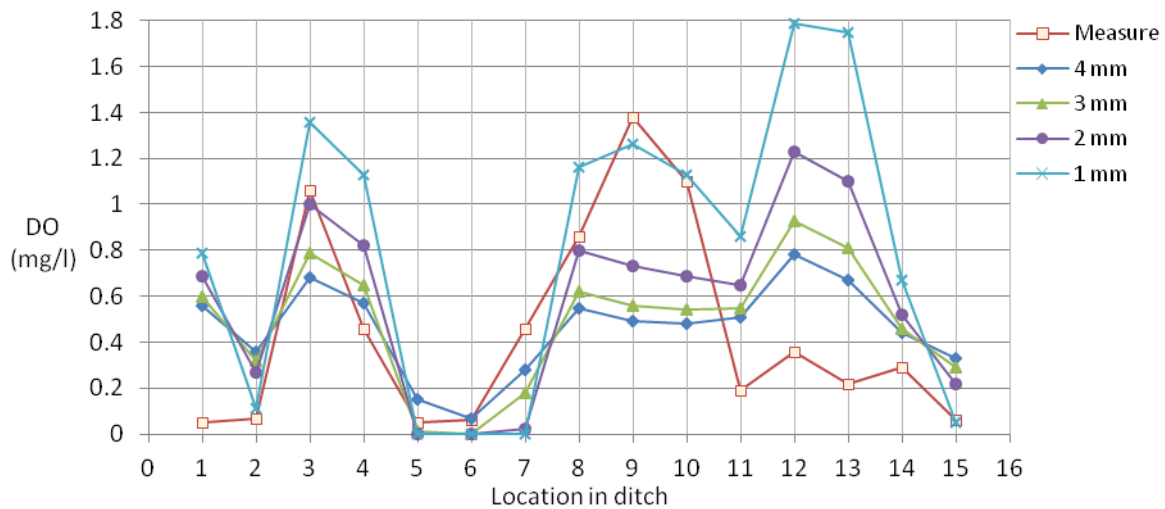
Fig. 16 - Calculated vs. measured dissolved oxygen with BOD distribution at different mean bubble sizes.

3.8   Discussion

3.8.1 CFD modelling

The accuracy of the CFD model is evaluated by comparison with site measurement data. Modelling the effect of BOD predicts the right level of DO. There is good agreement between the simulation and the physical observation in terms of the flow pattern and the mean DO, but not for the variation of DO. The BOD distribution improves the accuracy by better agreement with the measurements of variation of DO. The bubble size distribution (BSD) improves the accuracy by better agreement with the measurements of mean DO. The BSD predicts a mean bubble size of 1.9 mm, that agrees with the best agreement with the measurements. Therefore the BSD seems to predict the right mean bubble size. The study shows that the DO is affected by various parameters and therefore it is important to use the correct physical data. The CFD model can be used as a powerful tool to assess the aeration performance of an oxidation ditch.

Measures can be taken to try to improve the accuracy of the CFD model. Local refinement of the mesh close to the aerators may improve the accuracy. Quantifying accurately the oxygen transfer rate of the surface aerators by experimental measurement is useful. Including the transfer of atmospheric air through the water surface can be implemented in an oxygen source term. To predict the disturbance of the water surface the volume of fluid (VOF) surface tracking model may be used. The most significant change would be to consider three phase (gas-liquid-solid) flow. Tracer testing on the full-scale ditch can be used to validate the residence time distribution. The bubble size distribution may be helpful in understanding the different bubble sizes that are produced by the aerators. Bubble size measurements can also be undertaken. This would help validate the BSD and may be used for data for the bubble sizes at the inlets of the aerators.

3.8.2 Aeration design

The benefits to the aeration design are as follows. For all the aeration devices there is an increase in water velocity which can mitigate against sludge deposition. The jet aerator and surface aerators provide a dominant flow direction which reduces flow short circuiting. For all the devices there is an increase in ditch residence time. *The drawbacks to the aeration design are as follows.* The main cause of heterogeneous flow distribution is the jet aerator. The jet aerator causes the flow from the surface aerators to become asymmetric. The surface aerators produce undesirable heterogeneous vertical flow distribution. The oxygen transfer rate of the surface aerators is difficult to quantify unless it is measured. The diffusion aerator produces undesirable local flow recirculation.

The CFD model can be used to optimise the design of the ditch and aeration devices. The optimal design is to improve the uniformity of the flow pattern and DO distribution, increase the residence time and reduce the energy consumption. Aerators can be optimised individually in terms of their number, position, orientation, water flow rate and oxygen supply. Possible design cases can be for the optimum rotating speed of the surface aerator and the pore size of the membrane diffuser. Design recommendations from the literature can be used, although care must be taken because they always have a unique design scenario. The energy requirements of the aerators can be calculated for each possible design scenario. This can then be used in order to conduct a cost (energy) to benefit (aeration) analysis.

4. Conclusions

This paper predicts the gas-liquid flow pattern and dissolved oxygen distribution in a wastewater treatment oxidation ditch with various aeration devices. The study considers the effects of BOD distribution, bubble size distribution and other parameters on the distribution of dissolved oxygen. Predictions are evaluated by the comparison between computation and on-site experimentation. CFD modelling of gas-liquid flow and species transport of DO and BOD is undertaken. The input uniform mean bubble size is an average value from the CFD models in literature.

Without the aeration devices the flow behaviour in the ditch is mostly plug flow. The jet aerator, membrane diffuser and surface aerators increase the flow velocities and cause undesirable heterogeneous flow distribution. However, the hydraulic residence time in the ditch is beneficially increased by the aeration devices.

To predict the dissolved oxygen distribution, the oxygen scalar equation has a source term for aeration and a sink term for the oxygen consumption by BOD. The BOD distribution is modelled as a heterogeneous oxygen sink, unlike previous CFD models that simplify it by using a uniform BOD. The uniform and distributed BOD predict similar mean and maximum DO concentrations, but have differences in the variation of DO. The dissolved oxygen is affected by temperature, surface aeration, bubble size, BSD, molar fraction Henry coefficient, mass diffusivity and turbulent Schmidt number of oxygen in water.

There is good agreement between the predictions and the physical observations in terms of the flow pattern. The comparison between the predicted mean DO and the measurements show good quantitative agreement. The variation of DO in the ditch shows better agreement when there is a BOD distribution. The nearest match to the measurements is a 2 mm bubble size, that agrees with the mean bubble size of 1.9 mm that is predicted by the BSD. This study identifies that the BOD distribution and BSD are important parameters and are also current gaps in research. The study identifies ways in which the CFD model can be improved. The study also considers how the CFD model can be used to improve the design of the oxidation ditch and the aeration devices.

Acknowledgments

References

Brannock, M.W.D., 2003. Computational fluid dynamics tools for the design of mixed anoxic wastewater treatment vessels. PhD thesis. University Queensland, Australia.

Çengel, Y.A. and Boles, M.A., 2008. Thermodynamics: an engineering approach, McGraw-Hill.

Climent, J., Martínez-Cuenca, R., Carratalà, P., González-Ortega, M.J., Abellán, M., Monrós, G. and Chiva, S., 2019. A comprehensive hydrodynamic analysis of a full-scale oxidation ditch using population balance modelling in CFD simulation. *Chemical Engineering Journal*, 374, 760-775.

Cockx, A., Do-Quang, Z., Audic, J.M., Liné, A. and Roustan, M., 2001. Global and local mass transfer coefficients in waste water treatment process by computational fluid dynamics. *Chemical Engineering and Processing: Process Intensification*, 40(2), 187-194.

Degremont, G. ed., 2007, *Water treatment handbook*. John Wiley & Sons 11th Edition.

Dhanasekharan, K.M., Sanyal, J., Jain, A. and Haidari, A., 2005. A generalized approach to model oxygen transfer in bioreactors using population balances and computational fluid dynamics. *Chemical Engineering Science*, 60(1), 213-218.

Fan, L., Xu, N., Wang, Z. and Shi, H., 2010. PDA experiments and CFD simulation of a lab-scale oxidation ditch with surface aerators. *Chemical Engineering Research and Design*, 88(1), 23-33.

Fayolle, Y., Gillot, S., Cockx, A., Roustan, M. and Héduit, A., 2006. In situ local parameter measurements for CFD modelling to optimize aeration. *In Proceedings of the Water Environment Federation*, 9, 3314-3326.

Fayolle, Y., Cockx, A., Gillot, S., Roustan, M. and Héduit, A., 2007. Oxygen transfer prediction in aeration tanks using CFD. *Chemical Engineering Science*, 62(24), 7163-7171.

Frank, T., Zwart, P.J., Shi, J.M., Krepper, E., Lucas, D. and Rohde, U., 2005, September. Inhomogeneous MUSIG model - A population balance approach for polydispersed bubbly flows. In *Proceeding of International Conference for Nuclear Energy for New Europe, Bled, Slovenia*.

Ghawi, A.H., 2014. Performance improvement of conventional aeration tanks using CFD modelling. *Kufa journal of Engineering*, *3*(1).

Gillot, S. and Heduit, A., 2000. Effect of air flow rate on oxygen transfer in an oxidation ditch equipped with fine bubble diffusers and slow speed mixers. *Water Research*, 34(5), 1756-1762.

Gresch, M., Braun, D. and Gujer, W., 2010. The role of the flow pattern in wastewater aeration tanks. *Water Science and Technology*, 61(2), 407-414.

Gresch, M., Armbruster, M., Braun, D. and Gujer, W., 2011. Effects of aeration patterns on the flow field in wastewater aeration tanks. *Water research*, 45(2), 810-818.

Guo, X., Zhou, X., Chen, Q. and Liu, J., 2013. Flow field and dissolved oxygen distributions in the outer channel of the Orbal oxidation ditch by monitor and CFD simulation. *Journal of Environmental Sciences*, 25(4), 645-651.

Higbie, R., 1935. The rate of absorption of a pure gas into a still liquid during short periods of exposure. *Trans. AIChE*, 31, 365-389.

Höhne, T. and Mamedov, T., 2020. CFD Simulation of Aeration and Mixing Processes in a Full-Scale Oxidation Ditch. *Energies*, *13*(7), p.1633.

Hreiz, R., Potier, O., Wicks, J. and Commenge, J.M., 2019. CFD Investigation of the effects of bubble aerator layouts on hydrodynamics of an activated sludge channel reactor. *Environmental technology*, *40*(20), pp.2657-2670.

Hu, Y., Guo, Y., Zhu, W. and Chen, B., 2010, June. Numerical simulation and experiment of gas-liquid flow in aeration tanks. In *2010 International Conference on Mechanic Automation and Control Engineering (MACE),* 2140-2144. IEEE.

Huang, W., Wu, C. and Xia, W., 2009. Oxygen transfer in high-speed surface aeration tank for wastewater treatment: full-scale test and numerical modelling. *Journal of Environmental Engineering*, 135(8), 684-691.

Ishii, M. and Zuber, N., 1979. Drag coefficient and relative velocity in bubbly, droplet or particulate flows. *AIChE Journal*, 25(5), 843-855.

Karpinska, A.M., Dias, M.M., Boaventura, R.R., Lopes, J.C.B., Santos, R.J., 2010. CFD approach on the energy analysis of an oxidation ditch aerated with hydrojets. *In World Congress on Water, Climate and Energy.*

Karpinska Portela, A.M., 2013. *New design tools for activated sludge process*. PhD Thesis. FEUP, University of Porto, Porto, Portugal.

Karpinska, A.M., Dias, M.M., Boaventura, R.A. and Santos, R.J., 2015. Modelling of the hydrodynamics and energy expenditure of oxidation ditch aerated with hydrojets using CFD codes. *Water Quality Research Journal of Canada*, 50(1), 83-94.

Karpinska, A.M. and Bridgeman, J., 2016. CFD aided modelling of activated sludge systems - a critical review. *Water Research*, 88(10), 861-879.

Karpinska, A.M. and Bridgeman, J., 2017. Towards a robust CFD model for aeration tanks for sewage treatment - a lab-scale study. *Engineering Applications of Computational Fluid Mechanics*, 11(1), 371-395.

Karpinska, A.M. and Bridgeman, J., 2018. CFD as a tool to optimize aeration tank design and operation. *Journal of Environmental Engineering*, *144*(2), p.05017008.

Launder, B.E. and Spalding, D.B., 1974. The numerical computation of turbulent flows. *Computer Methods in Applied Mechanics and Engineering*, 3(2), 269-289.

Lei, L. and Ni, J., 2014. Three-dimensional three-phase model for simulation of hydrodynamics, oxygen mass transfer, carbon oxidation, nitrification and denitrification in an oxidation ditch. *Water Research*, 53, 200-214.

Le Moullec, Y., Potier, O., Gentric, C. and Leclerc, J.P., 2008. Flow field and residence time distribution simulation of a cross-flow gas–liquid wastewater treatment reactor using CFD. *Chemical Engineering Science*, 63(9), 2436-2449.

Le Moullec, Y., Gentric, C., Potier, O. and Leclerc, J.P., 2010. CFD simulation of the hydrodynamics and reactions in an activated sludge channel reactor of wastewater treatment. *Chemical Engineering Science*, 65(1), 492-498.

Littleton, H.X., Daigger, G.T. and Strom, P.F., 2007. Application of computational fluid dynamics to closed-loop bioreactors: I. Characterization and simulation of fluid-flow pattern and oxygen transfer. *Water Environment Research*, 79(6), 600-612.

Liu, Y.L., Wei, W.L., Lv, B. and Yang, X.F., 2014. Research on optimal radius ratio of impellers in an oxidation ditch by using numerical simulation. *Desalination and Water Treatment*, 52(13-15), 2811-2816.

Lo, S., 1998. *Modelling of bubble breakup and coalescence with the MUSIG model.* Report. AEA Technology, UK, 1-17.

Luo, H. and Svendsen, H.F., 1996. Theoretical model for drop and bubble breakup in turbulent dispersions. *AIChE Journal*, 42(5), 1225-1233.

McWhirter, J.R., Chern, J.M. and Hutter, J.C., 1995. Oxygen mass transfer fundamentals of surface aerators. *Industrial & Engineering Chemistry Research*, 34(8), 2644-2654.

Nauman, E.B., 2007. *Residence Time Distributions.* John Wiley & Sons, Inc., New Jersey, NJ, USA, 535-574.

Nopens, I., Torfs, E., Ducoste, J., Vanrolleghem, P.A. and Gernaey, K.V., 2015. Population balance models: a useful complementary modelling framework for future WWTP modelling. *Water Science and Technology*, 71(2), 159-167.

Potier, O., Leclerc, J.P. and Pons, M.N., 2005. Influence of geometrical and operational parameters on the axial dispersion in an aerated channel reactor. *Water Research*, 39(18), 4454-4462.

Pope, S.B., 2000. *Turbulent flows.* Cambridge University Press, Cambridge, UK.

Ranade, V.V., 2002, *Computational flow modelling for chemical reactor engineering.* Academic Press. San Diego, CA.

Ratkovich, N., 2010. *Understanding hydrodynamics in membrane bioreactor systems for wastewater treatment: Two-phase empirical and numerical modelling and experimental validation.* PhD Thesis, Faculty of Bioscience Engineering, University of Ghent, Belgium.

Rodi, W., 1993. *Turbulence Models and Their Application in Hydraulics*. CRC Press.

Roman, M.D. and Felseghi, R.A., 2014. Analysis of oxygen transfer and dissolved oxygen concentration measurement tests in a wastewater treatment plant. In *Applied Mechanics and Materials* (Vol. 656, pp. 486-494). Trans Tech Publications.

Rosso D., Stenstrom M.K., and Larson L.E., 2008. Aeration of large-scale municipal wastewater treatment plants: state of the art. *Water Science and Technology,* 57(7), 973-78.

Samstag, R.W., Ducoste, J.J., Griborio, A., Nopens, I., Batstone, D.J., Wicks, J.D., Saunders, S., Wicklein, E.A., Kenny, G. and Laurent, J., 2016. CFD for wastewater treatment: an overview. *Water Science and Technology*, 74(3), 549-563.

Talvy, S., Cockx, A. and Line, A., 2007. Modelling hydrodynamics of gas–liquid airlift reactor. *AIChE journal*, 53(2), 335-353.

Terashima, M., So, M., Goel, R. and Yasui, H., 2016. Determination of diffuser bubble size in computational fluid dynamics models to predict oxygen transfer in spiral roll aeration tanks. *Journal of Water Process Engineering*, 12, 120-126.

Thakre, S.B., Bhuyar, L.B. and Deshmukh, S.J., 2008. Effect of different configurations of mechanical aerators on oxygen transfer and aeration efficiency with respect to power consumption. *International Journal of Aerospace and Mechanical Engineering*, 2(2), 100-108.

Wang, H., Li, Y. and Zhao, Z., 2009. Computational study on micro-scale behaviour of bubble generated by aeration in a plug-flow aeration tank. *Water Science and Technology*, 59(10), 2065-2072.

Wei, W., Liu, Y. and Lv, B., 2016. Numerical simulation of optimal submergence depth of impellers in an oxidation ditch. *Desalination and Water Treatment*, 57(18), 8228-8235.

Wicklein, E., Batstone, D.J., Ducoste, J., Laurent, J., Griborio, A., Wicks, J., Saunders, S., Samstag, R., Potier, O. and Nopens, I., 2016. Good modelling practice in applying computational fluid dynamics for WWTP modelling. *Water Science and Technology*, 73(5), 969-982.

Xie, H., Yang, J., Hu, Y., Zhang, H., Yang, Y., Zhang, K., Zhu, X., Li, Y. and Yang, C., 2014. Simulation of flow field and sludge settling in a full-scale oxidation ditch by using a two-phase flow CFD model. *Chemical Engineering Science*, 109, 296-305.

Xu, N., Fan, L., Pang, H. and Shi, H., 2010. Feasibility study and CFD-aided design for a new type oxidation ditch based on airlift circulation. *The Canadian Journal of Chemical Engineering*, 88(5), 728-741.

Xu, Q., Yang, J., Hou, H., Hu, Y., Liang, S., Xiao, K., Wu, X., Liu, B., Hu, J., Hu, J. and Yang, C., 2018. Simulation of flow field and gas hold-up of a pilot-scale oxidation ditch by using a liquid-gas CFD model. *Water Science and Technology, 78(9),* pp.1956-1965.

Yang, Y., Wu, Y., Yang, X., Zhang, K. and Yang, J., 2010. Flow field prediction in full-scale Carrousel oxidation ditch by using computational fluid dynamics. *Water Science and Technology*, 62(2), 256-265.

Yang, Y., Yang, J., Zuo, J., Li, Y., He, S., Yang, X. and Zhang, K., 2011. Study on two operating conditions of oxidation ditch for optimisation of energy consumption and effluent quality by using CFD model. *Water Research*, 45(11), 3439-3452.

Zhang, Y., Zheng, Y., Fernandez-Rodriguez, E., Yang, C., Zhu, Y., Liu, H. and Jiang, H., 2016. Optimization design of submerged propeller in oxidation ditch by computational fluid dynamics and comparison with experiments. *Water Science and Technology*, 74(3), 681-690.

Zhang, Y., Li, C., Xu, Y., Tang, Q., Zheng, Y., Liu, H. and Fernandez-Rodriguez, E., 2019. Study on propellers distribution and flow field in the oxidation ditch based on two-phase CFD model. *Water*, *11*(12), p.2506.